DTU Library

Multi-milliwatt mid-infrared supercontinuum generation in a suspended core chalcogenide fiber

Møller, Uffe Visbech; Yu, Yi; Kubat, Irnis; Petersen, Christian Rosenberg; Gai, Xin; Brilland, Laurent; Méchin, David; Caillaud, Celine; Troles, Johann; Luther-Davies, Barry

Total number of authors:
11

Published in:
Optics Express

Link to article, DOI:
10.1364/OE.23.003282

Publication date:
2015

Document Version
Publisher's PDF, also known as Version of record

Citation (APA):
Møller, U. V., Yu, Y., Kubat, I., Petersen, C. R., Gai, X., Brilland, L., Méchin, D., Caillaud, C., Troles, J., Luther-Davies, B., & Bang, O. (2015). Multi-milliwatt mid-infrared supercontinuum generation in a suspended core chalcogenide fiber. *Optics Express*, *23*(3), 3282-3291. https://doi.org/10.1364/OE.23.003282

Multi-milliwatt mid-infrared supercontinuum generation in a suspended core chalcogenide fiber

Uffe Møller,[1,*] Yi Yu,[2] Irnis Kubat,[1] Christian R. Petersen,[1] Xin Gai,[2] Laurent Brilland,[3] David Méchin,[3] Celine Caillaud,[4] Johann Troles,[4] Barry Luther-Davies,[2] and Ole Bang[1,5]

[1] *DTU Fotonik, Department of Photonics Engineering, Technical University of Denmark, 2800 Kgs. Lyngby, Denmark*
[2] *Centre for Ultrahigh bandwidth Devices for Optical Systems , Laser Physics Centre, Australian National University, Canberra, ACT 0200, Australia*
[3] *Perfos, R&D Platform of Photonics Bretagne, 11 Rue Louis de Broglie, 22300 Lannion, France*
[4] *Institut des Sciences Chimiques de Rennes, Equipe Verres et Céramiques, Université de Rennes 1, 35042 Rennes Cedex, France*
[5] *NKT Photonics A/S, Blokken 84, 3460 Birkerød, Denmark*

*ufmo@fotonik.dtu.dk

Abstract: A low-loss suspended core $As_{38}Se_{62}$ fiber with core diameter of 4.5 μm and a zero-dispersion wavelength of 3.5 μm was used for mid-infrared supercontinuum generation. The dispersion of the fiber was measured from 2.9 to 4.2 μm and was in good correspondence with the calculated dispersion. An optical parametric amplifier delivering 320 fs pulses with a peak power of 14.8 kW at a repetition rate of 21 MHz was used to pump 18 cm of suspended core fiber at different wavelengths from 3.3 to 4.7 μm. By pumping at 4.4 μm with a peak power of 5.2 kW coupled to the fiber a supercontinuum spanning from 1.7 to 7.5 μm with an average output power of 15.6 mW and an average power >5.0 μm of 4.7 mW was obtained.

OCIS codes: (320.6629) Supercontinuum generation; (190.4370) Nonlinear optics, fibers; (160.4330) Nonlinear optical materials; (060.4005) Microstructured fibers.

References and links

1. A. Schliesser, N. Picqué, and T. W. Hänsch, "Mid-infrared frequency combs," Nat. Photonics **6**, 440–449 (2012).
2. R. Wilson and H. Tapp, "Mid-infrared spectroscopy for food analysis: recent new applications and relevant developments in sample presentation methods," TRAC-Trend. Anal. Chem. **18**, 85–93 (1999).
3. P. Werle, F. Slemr, and K. Maurer, "Near-and mid-infrared laser-optical sensors for gas analysis," Opt. Laser. Eng. **37**, 101–114 (2002).
4. B. Guo, Y. Wang, C. Peng, H. Zhang, G. Luo, H. Le, C. Gmachl, D. Sivco, M. Peabody, and A. Cho, "Laser-based mid-infrared reflectance imaging of biological tissues," Opt. Express **12**, 208–219 (2004).
5. N. Savage,"Supercontinuum sources," Nat. Photonics **3**, 114–115 (2009).
6. P. Domachuk, N. A. Wolchover, M. Cronin-Golomb, A. Wang, A. K. George, C. M. B. Cordeiro, J. C. Knight, and F. G. Omenetto, "Over 4000 nm bandwidth of mid-IR supercontinuum generation in sub-centimeter segments of highly nonlinear tellurite PCFs," Opt. Express **16**, 7161–7168 (2008).
7. G. Qin, X. Yan, C. Kito, M. Liao, C. Chaudhari, T. Suzuki, and Y. Ohishi, Yasutake, "Ultrabroadband supercontinuum generation from ultraviolet to 6.28μm in a fluoride fiber," Appl. Phys. Lett. **95**, 161103 (2009).
8. C. Xia, Z. Xu, M. N. Islam, F. L. Terry, M. J. Freeman, A. Zakel, and J. Mauricio, "10.5 W time-averaged power did-IR supercontinuum generation extending beyond 4 μm with direct pulse pattern modulation," IEEE J. Sel. Top. Quant. **15**, 422–434 (2009).

9. R. Buczynski, H. Bookey, M. Klimczak, D. Pysz, R. Stepien, T. Martynkien, J. McCarthy, A. Waddie, A. Kar, and M. R. Taghizadeh, "Two Octaves Supercontinuum generation in lead-bismuth glass based photonic crystal fiber," Materials **7**, 4658–4668 (2014).
10. B. J. Eggleton, B. Luther-Davies, and K. Richardson, "Chalcogenide photonics," Nat. Photonics **5**, 141–148 (2011).
11. J. M. Dudley and J. R. Taylor, "Ten years of nonlinear optics in photonic crystal fibre," Nat. Photonics **3**, 85–90 (2009).
12. P. M. Moselund, C. Petersen, S. Dupont, C. Agger, O. Bang, and S. R. Keiding, "Supercontinuum: broad as a lamp, bright as a laser, now in the mid-infrared," Proc. SPIE **8381**, 83811A (2012).
13. R. Thapa, D. Rhonehouse, D. Nguyen, K. Wiersma, C. Smith, J. Zong, and A. Chavez-Pirson, "Mid-IR supercontinuum generation in ultra-low loss, dispersion-zero shifted tellurite glass fiber with extended coverage beyond 4.5 μm," Proc. SPIE **8898**, 889808 (2013).
14. C. Markos, I. Kubat, and O. Bang, "Hybrid polymer photonic crystal fiber with integrated chalcogenide glass nanofilms," Sci. Rep. **4**, 06057 (2014).
15. V. Shiryaev and M. Churbanov, "Trends and prospects for development of chalcogenide fibers for mid-infrared transmission," J. Non-Cryst. Solids **377**, 225–230 (2013).
16. R. E. Slusher, G. Lenz, J. Hodelin, J. Sanghera, L. B. Shaw, and I. D. Aggarwal, "Large Raman gain and nonlinear phase shifts in high-purity As2Se3 chalcogenide fibers," J. Opt. Soc. Am. B **21**, 1146 (2004).
17. H. G. Dantanarayana, N. Abdel-Moneim, Z. Tang, L. Sojka, S. Sujecki, D. Furniss, A. B. Seddon, I. Kubat, O. Bang, and T. M. Benson, "Refractive index dispersion of chalcogenide glasses for ultra-high numerical-aperture fiber for mid-infrared supercontinuum generation," Opt. Mat. Express **4**, 1444–1455 (2014).
18. I. Kubat, C. S. Agger, U. Møller, A. B. Seddon, Z. Tang, S. Sujecki, T. M. Benson, D. Furniss, S. Lamrini, K. Scholle, P. Fuhrberg, B. Napier, M. Farries, J. Ward, P. M. Moselund, and O. Bang, "Mid-infrared supercontinuum generation to 12.5μm in large NA chalcogenide step-index fibres pumped at 4.5μm," Opt. Express **22**, 19169–19182 (2014).
19. D. D. Hudson, M. Baudisch, D. Werdehausen, B. J. Eggleton, and J. Biegert, "1.9 octave supercontinuum generation in a As_2S_3 step-index fiber driven by mid-IR OPCPA," Opt. Lett. **39**, 5752–5755 (2014).
20. F. Théberge, N. Thiré, J.-F. Daigle, P. Mathieu, B. E. Schmidt, Y. Messaddeq, R. Vallée, and F. Légaré, "Multi-octave infrared supercontinuum generation in large-core As_2S_3 fibers," Opt. Lett. **39**, 6474 (2014).
21. C. R. Petersen, U. Møller, I. Kubat, B. Zhou, S. Dupont, J. Ramsay, T. Benson, S. Sujecki, N. Abdel-Moneim, Z. Tang, D. Furniss, A. Seddon, and O. Bang, "Mid-IR supercontinuum covering the molecular fingerprint region from 2 μm to 13 μm using ultra-high NA chalcogenide step-index fibre," Nat. Photonics **8**, 830–834 (2014).
22. A. Al-kadry, C. Baker, M. El Amraoui, Y. Messaddeq, and M. Rochette, "Broadband supercontinuum generation in As2Se3 chalcogenide wires by avoiding the two-photon absorption effects," Opt. Lett. **38**, 1185–1187 (2013).
23. O. Mouawad, J. Picot-Clémente, F. Amrani, C. Strutynski, J. Fatome, B. Kibler, F. Désévédavy, G. Gadret, J.-C. Jules, D. Deng, Y. Ohishi, and F. Smektala, "Multioctave midinfrared supercontinuum generation in suspended-core chalcogenide fibers," Opt. Lett. **39**, 2684–2687 (2014).
24. T. Cheng, Y. Kanou, X. Xue, D. Deng, M. Matsumoto, T. Misumi, T. Suzuki, and Y. Ohishi, "Mid-infrared supercontinuum generation in a novel AsSe_2-As_2S_5 hybrid microstructured optical fiber," Opt. Express **22**, 23019–23025 (2014).
25. I. Kubat, C. R. Petersen, U. V. Møller, A. Seddon, T. Benson, L. Brilland, D. Méchin, David P. M. Moselund, and O. Bang, "Thulium pumped mid-infrared 0.9-9μm supercontinuum generation in concatenated fluoride and chalcogenide glass fibers," Opt. Express **22**, 3959–3967 (2014).
26. Y. Yu, X. Gai, P. Ma, D.-Y. Choi, Z. Yang, R. Wang, S. Debbarma, S. Madden, and B. Luther-Davies, "A broadband, quasi-continuous, mid-infrared supercontinuum generated in a chalcogenide glass waveguide," Laser Photon. Rev. **8**, 792–798 (2014).
27. M. Liao, W. Gao, T. Cheng, X. Xue, Z. Duan, D. Deng, H. Kawashima, T. Suzuki, and Y. Ohishi, "Five-octave-spanning supercontinuum generation in fluoride glass," Appl. Phys. Express **6**, 032503 (2013).
28. J. J. Pigeon, S. Y. Tochitsky, C. Gong, and C. Joshi, "Supercontinuum generation from 2 to 20 μm in GaAs pumped by picosecond CO_2 laser pulses," Opt. Lett. **39**, 3246–3249 (2014).
29. Q. Coulombier, L. Brilland, P. Houizot, T. Chartier, T. N. N'Guyen, F. Smektala, G. Renversez, A. Monteville, D. Méchin, T. Pain, H. Orain, J.-C. Sangleboeuf, and J. Trolès, "Casting method for producing low-loss chalcogenide microstructured optical fibers," Opt. Express **18**, 9107–9112 (2010).
30. M. D. Nielsen, G. Vienne, J. R. Folkenberg, and A. Bjarklev, "Investigation of microdeformation-induced attenuation spectra in a photonic crystal fiber," Opt. Lett. **28**, 236–238 (2003).
31. N. A. Mortensen and J. R. Folkenberg, "Low-loss criterion and effective area considerations for photonic crystal fibres," J. Opt. A - Pure Appl. Opt. **5**, 163–167 (2003).
32. P. Roberts, F. Couny, H. Sabert, B. Mangan, T. Birks, J. Knight, and P. Russell, "Loss in solid-core photonic crystal fibers due to interface roughness scattering," Opt. Express **13**, 7779–7793 (2005).
33. J. Troles, Q. Coulombier, G. Canat, M. Duhant, W. Renard, P. Toupin, L. Calvez, G. Renversez, F. Smektala, M. El Amraoui, J. L. Adam, T. Chartier, D. Mechin, and L. Brilland, "Low loss microstructured chalcogenide fibers for large non linear effects at 1995 nm," Opt. Express **18**, 26647–26654 (2010).

#221338 - $15.00 USD Received 3 Dec 2014; revised 15 Jan 2015; accepted 28 Jan 2015; published 4 Feb 2015

34. J. Adam, J. Trolès, and L. Brilland, "Low-loss mid-IR microstructured optical fibers," in *Optical Fiber Communication Conference*, OSA Technical Digest (Optical Society of America, 2012), paper OM3D.2.
35. J. M. Dudley, G. Genty, and S. Coen, "Supercontinuum generation in photonic crystal fiber," Rev. Mod. Phys. **78**, 1135–1184 (2006).
36. S. T. Sørensen, U. Møller, C. Larsen, P. M. Moselund, C. Jakobsen, J. Johansen, T. V. Andersen, C. L. Thomsen, and O. Bang, "Deep-blue supercontinnum sources with optimum taper profiles verification of GAM," Opt. Express **20**, 10635–10645 (2012).
37. M. Frosz, P. Falk, and O. Bang, "The role of the second zero-dispersion wavelength in generation of supercontinua and bright-bright soliton-pairs across the zero-dispersion wavelength," Opt. Express **13**, 6181–6192 (2005).
38. Amorphous Materials Inc., "AMTIR-2," (2014). Online at http://www.amorphousmaterials.com/.
39. C. Caillaud, G. Renversez, L. Brilland, D. Mechin, L. Calvez, J.-L. Adam, and J. Troles, "Photonic Bandgap Propagation in All-Solid Chalcogenide Microstructured Optical Fibers," Materials **7**, 6120–6129 (2014).
40. D. Deng, D. Sega, T. Cheng, W. Gao, X. Xue, T. Suzuki, and Y. Ohishi, "Dispersion characterization of two orthogonal modes in a birefringence tellurite microstructured optical fiber," Opt. Express **22**, 23920–23927 (2014).
41. P. Hlubina, M. Kadulová, and D. Ciprian, "Spectral interferometry-based chromatic dispersion measurement of fibre including the zero-dispersion wavelength," J. Eur. Opt. Soc, Rapid Publ. **7**, 12017 (2012).
42. M. H. Frosz, "Validation of input-noise model for simulations of supercontinuum generation and rogue waves," Opt. Express **18**, 14778–14787 (2010).
43. C. Agger, C. Petersen, S. Dupont, H. Steffensen, J. K. Lyngsø, C. L. Thomsen, J. Thøgersen, S. R. Keiding, and O. Bang, "Supercontinuum generation in ZBLAN fibers - detailed comparison between measurement and simulation," J. Opt. Soc. Am. B **29**, 635–645 (2012).
44. E. A. Romanova, Y. S. Kuzyutkina, A. I. Konyukhov, N. Abdel-Moneim, A. B. Seddon, T. M. Benson, S. Guizard, and A. Mouskeftaras, "Nonlinear optical response and heating of chalcogenide glasses upon irradiation by the ultrashort laser pulses," Opt. Eng. **53**, 071812 (2014).
45. B. Ung and M. Skorobogatiy, "Chalcogenide microporous fibers for linear and nonlinear applications in the mid-infrared," Opt. Express **18**, 8647–8659 (2010).
46. F. Poletti and P. Horak, "Dynamics of femtosecond supercontinuum generation in multimode fibers," Opt. Express **17**, 6134–6147 (2009).
47. I. Shavrin, S. Novotny, and H. Ludvigsen, "Mode excitation and supercontinuum generation in a few-mode suspended-core fiber," Opt. Express **21**, 32141–32150 (2013).
48. S. Coen, A. H. L. Chau, R. Leonhardt, J. D. Harvey, J. C. Knight, W. J. Wadsworth, and P. S. J. Russell, "Supercontinuum generation by stimulated Raman scattering and parametric four-wave mixing in photonic crystal fibers," J. Opt. Soc. Am. B **19**, 753–764 (2002).
49. R. Khakimov, I. Shavrin, S. Novotny, M. Kaivola, and H. Ludvigsen, "Numerical solver for supercontinuum generation in multimode optical fibers," Opt. Express **21**, 14388–14398 (2013).

1. Introduction

The mid-infrared spectral region is of great interest because virtually all organic compounds display distinctive spectral fingerprints therein that reveal information about their chemical structure [1]. The mid-infrared region is, therefore, of key importance to many applications including food quality control [2], gas sensing [3] and medical diagnostics [4]. Supercontinuum laser sources spanning the visible and near-infrared based on optical nonlinear effects in tailored photonic crystal fibers (PCFs) are now commercially available [5]. However, the use of silica fibers as the generating medium has its limitations: the material absorption of silica increases drastically at wavelengths beyond $\sim$2 μm and this effectively prevents the spectral evolution of the supercontinuum generation (SCG) into the mid-infrared. Research into other nonlinear materials that can open the door to the mid-infrared spectral region has intensified in recent years. Several non-silica materials have been proposed as candidates for mid-infrared fibers, including tellurite [6], fluoride [7, 8], heavy metal oxide [9] and chalcogenide based materials [10]. However, the change of nonlinear material will inevitably change the fiber properties. Generally, efficient and broadband SCG is obtained by pumping close to the zero dispersion wavelength (ZDW) of the fiber. Silica fibers, especially PCFs, can be designed to have their ZDW at the wavelength of commercially available fiber lasers, such as ytterbium (1.06 μm) or erbium lasers (1.55 μm) [11]. The current state-of-the art in supercontinuum sources covering the near to mid-infrared region of the spectrum is based on fluoride or tellurite fibers which cover the 1-4.75 μm spectral range [8, 12, 13]. Again, the material absorption at the

#221338 - $15.00 USD Received 3 Dec 2014; revised 15 Jan 2015; accepted 28 Jan 2015; published 4 Feb 2015

long wavelength edge dictates the upper limit. Chalcogenide glasses, on the other hand, have been shown to be promising candidates for highly-nonlinear photonic devices [10,14] including mid-infrared SCG as they can transmit light out to 25 μm [15] and they possess high nonlinear refractive indices, up to a factor of 1,000 more than silica [16]. For As_2Se_3 the ZDW of the material is around 7 μm, but it can be tailored using waveguide dispersion to $\sim 5\mu$m in a 10 μm core step-index As_2Se_3 fiber [17,18]. Recently, Hudson *et al.* generated a 1.6-5.9 μm SC in a step-index As_2S_3 fiber with a core diameter of 9 μm by pumping at 3.1 μm [19], Théberge *et al.* used a step-index As_2S_3 fiber with a 100 μm core to generate an SC spanning from 1.5 to 7.0 μm by pumping at 4.56 μm based on self-focusing and beam filamentation [20], and Petersen *et al.* used 100 fs pulses at 6.3 μm to generate SC spanning from 1.4 to 13.3 μm in 85 mm of ultra high NA As_2Se_3 step-index fiber with a 16 μm core [21]. Al-kadry *et al.* shifted the ZDW all the way down to 1.73 μm by tapering an As_2Se_3 fiber down to a diameter of 1.28 μm [22]. However, tapering to small dimensions comes with the cost of power handling and the second ZDW may eventually limit the SCG at longer wavelengths. An alternative approach to shift the ZDW to shorter wavelengths is to fabricate microstructured optical fibers (MOFs). Mouawad *et al.* succeeded in generating supercontinuum from 0.6 to 4.1 μm in an As_2S_3 suspended core fiber with a core diameter of 3.4 μm pumped at 2.5 μm [23], and Cheng *et al.* demonstrated a supercontinuum spanning from 1.3 to 5.4 μm in an $AsSe_2$-As_2S_5 hybrid MOF [24]. Kubat *et al.* numerically demonstrated that by cascading a ZBLAN-based SC into a As_2S_3 grapefruit MOF with a core diameter of 5 μm it is possible to generate SC out to 9 μm [25]. Other types of waveguides and bulk materials have also been used for SCG, and Yu *et al.* recently reported on a supercontinuum spanning from 1.8 to 7.5 μm in a chalcogenide rib waveguide with a 2.5 μm thick core layer [26]. Liao *et al.* obtained an SC from 0.39-7.4 μm at -20 dB in a 32 mm ZBLAN sample [27] and Pigeon *et al.* generated a 2-20 μm supercontinuum in a 67 mm GaAs sample by pumping with a CO_2 laser at 9.3 μm [28]. The drawback of using bulk samples for SCG is, however, the lack of confinement which will require higher power.

In this paper we present experimental results on SCG in a low-loss 18 cm $As_{38}Se_{62}$ suspended core fiber with a core diameter of 4.5 μm pumped at different wavelengths from 3.3 to 4.7 μm with 320 fs pulses from an optical parametric amplifier (OPA). Pumping at 4.4 μm with a peak power of 5.2 kW coupled to the fiber we obtained a supercontinuum spanning from 1.7-7.5 μm with an average output power of 15.6 mW and an average power $>$5.0 μm of 4.7 mW. When pumping at 4.7 μm we obtained an average output power of 16.0 mW and an average power $>$5.0 μm of 7.5 mW. However the supercontinuum did in this case contain dips below -20 dB and this limited the total bandwidth. This is to our knowledge the furthest into the mid-infrared reported in a chalcogenide MOF. The presented experiment is entirely reproducible using components that can be purchased and represents a practical solution for e.g. mid-infrared spectroscopy.

2. Experimental setup and optical parameters of fiber

The experimental setup is shown schematically in Fig. 1(a). The mid-infrared OPA consists of a high power pulsed Yb fs laser which is used to pump a 10 mm long PPLN crystal. A tunable semiconductor laser was used as a seed to generate light from 3.3-4.7 μm. The average output power of the mid-infrared OPA was up to 250 mW at 4 μm with a pulse duration of 320 fs at a repetition rate of 21 MHz [26]. However, for SCG the maximum power was set to 100 mW, which corresponds to a peak power of 14.8 kW. The light from the mid-infrared OPA was sent through a chopper and a polarizer pair in order to control the polarization and power. The light was coupled with an NA = 0.85 molded chalcogenide lens to the 18 cm long suspended core fiber with a core diameter of 4.5 μm . The output from the fiber was collected by either a similar molded lens for insertion loss measurements, or a reflective objective lens for spectroscopic

#221338 - $15.00 USD Received 3 Dec 2014; revised 15 Jan 2015; accepted 28 Jan 2015; published 4 Feb 2015

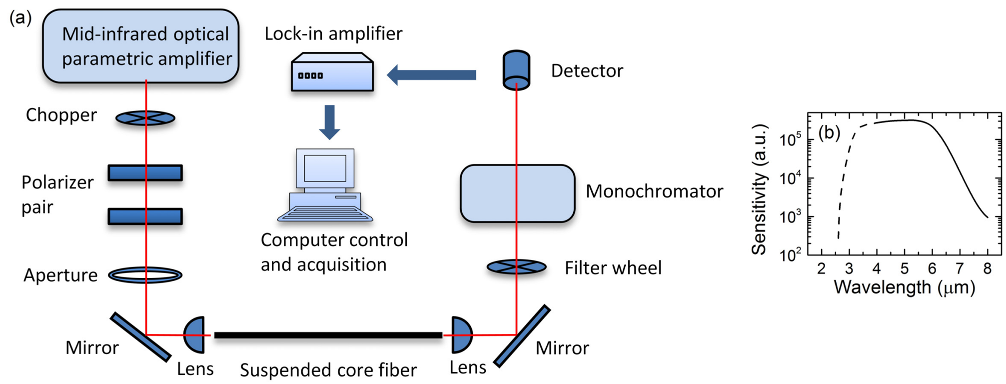

Fig. 1. (a) Schematic of the experimental setup. (b) MCT detector responsivity.

measurements that were performed using a Newport Cornerstone 1/4 m monochromator. Either a PbSe or a MCT detector connected to a lock-in amplifier was used to record the spectra in the range 1.5-4.0 μm and 4.0-8.5 μm, respectively. Filters were used to prevent higher order grating reflections from reaching the detectors. At wavelengths > 4.0 μm the data was corrected for the detector responsivity, which was provided by the manufacturer and shown in Fig. 1(b).

The total insertion loss of the fiber plus the coupling lenses was measured to be 7.5 dB and thus the power delivered to the fiber was estimated to be 3.75 dB lower than the measured average power after the chopper. This corresponds to 118 W of peak power delivered to the fiber for every mW of average power measured after the chopper.

The $As_{38}Se_{62}$ suspended core fiber had a core diameter of 4.5 μm and was manufactured by Perfos. The fiber has been fabricated by the molding technique described in [29]. A SEM image of the fiber is shown in Fig. 2(a). Core transmission up to 8 μm was verified in an

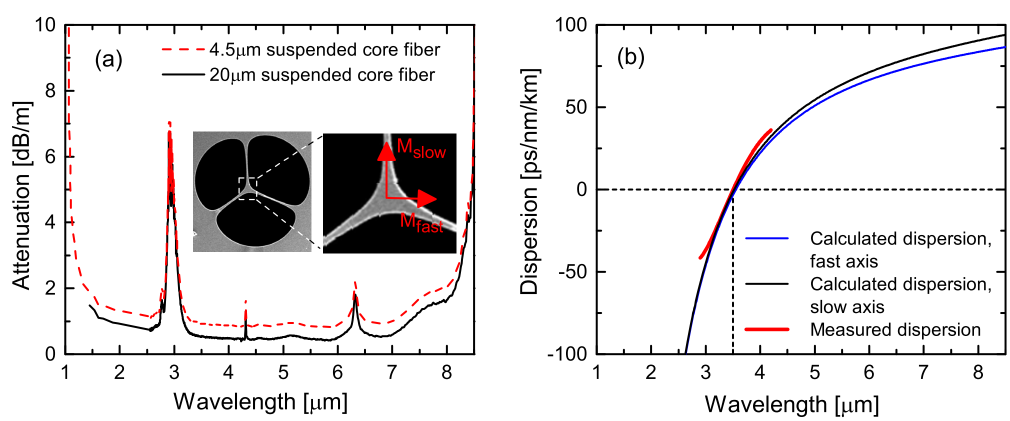

Fig. 2. Optical properties of the suspended core fiber. (a) Measured fiber loss of a 6-hole suspended core fiber with a core diameter of a 20 μm (black solid) and estimated fiber loss of a suspended core fiber with a core diameter of 4.5 μm (red dashed). Inset: SEM image of the 4.5 μm suspended core fiber and a zoom-in on the core indication the fast and slow polarization axis. (b) Measured (red) and calculated dispersion for the slow (black) and fast (blue) axis.

FTIR spectrometer, but due to the low intensity it was not possible to extract the loss from

#221338 - $15.00 USD Received 3 Dec 2014; revised 15 Jan 2015; accepted 28 Jan 2015; published 4 Feb 2015

this measurement. However, to estimate the loss of the 4.5 μm suspended core fiber, the fiber loss of a 6-hole suspended core fiber with a core diameter of 20 μm was measured by the cut-back method in an FTIR from 1.4-8.5 μm and shown as the solid black curve in Fig. 2(a). It has been shown that by decreasing the core size the fiber loss will increase due to micro-deformations [30–32]. Troles *et al.* characterized the fiber loss in $As_{38}Se_{62}$ microstructured optical fibers that are similar to the one used here. They found that a 3 μm suspended core fiber had a 0.4 dB higher loss than a 20 μm suspended core fiber at a wavelength of 1.55 μm [33]. Adam *et al.* measured the material loss of bulk As_2Se_3 similar to the material used for the 4.5 μm suspended core fiber, and the material transmission window was from 1 to 8.5 μm [34]. To estimate the loss of the 4.5 μm suspended core fiber we added 0.4 dB to the fiber loss measurement of the 20 μm suspended core fiber and extrapolated the loss in both ends of the transmission window at 1 and 10 μm to be 100 dB/m. The total estimated fiber loss of the 4.5 μm suspended core fiber is shown as the dashed red line in Fig. 2(a). The absorption band at 4.3 μm and the bands at 2.9 and 6.2 μm are due to Se-H and water pollution, respectively [33].

The fiber dispersion, and in particular the location of the ZDW, is of great importance for the SCG process [35–37]. Based on the fiber geometry provided by Perfos and the As_2Se_3 material refractive index measurements from Amorphous Materials Inc. [38], which were in good agreement with the refractive index of $As_{38}Se_{62}$ [39], the fiber dispersions of the slow and fast axis were calculated in COMSOL Multiphysics and are shown in Fig. 2(b). Because of its geometry, the fiber is slightly birefringent with a birefringence of $4.2 \cdot 10^{-4}$ at 3.5 μm. The effect of SCG in a birefringent fiber has been showed by Deng *et al.* [40], we did however not see any difference due to the fiber orientation neither when measuring the dispersion nor when generating supercontinuum. Thus, no special care was taken to orient the fiber to account for the birefringence. The fiber dispersion of the suspended core fiber was measured by means of spectral-domain white light interferometry using a ZBLAN-fiber-based supercontinuum source generating light from 1.5-4.5 μm. The dispersion measurement setup consisted of a balanced Mach-Zehnder interferometer wherein a 165 mm test fiber was placed in one arm and the reference arm could be varied in length by a translation stage. Matching the optical path delay of the two arms gives rise to an interference pattern. By fitting the position of fringe peaks and valleys to a modified Cauchy dispersion equation the dispersion of the fundamental mode can be extracted [41]. The measured dispersion from 2.9-4.2 μm, which represents the average over several measurements, is shown as the solid red curve in Fig. 2(b). There is a good agreement between the measured and calculated fiber dispersion. The measured ZDW was 3.50 μm while the calculated ZDW was 3.52 μm and 3.55 μm for the slow and fast axis, respectively.

3. Experimental results and simulations

Supercontinuum spectra at different input powers pumped at 3.3 μm and 3.5 μm are shown in Figs. 3(a) and 3(b), respectively. As expected the supercontinuum spectra are broadened for increasing powers both when pumping in the normal dispersion regime at 3.3 μm as well as at the ZDW at 3.5 μm.

The SCG was modelled using the generalized nonlinear Schrödinger equation (GNLSE) for single mode and single-polarization with a chirp-free Gaussian-shaped pump pulse as the initial condition. A one-photon-per-mode noise model was used to model the spectral fluctuations from shot to shot in the input pulse [35, 42]. The GNLSE was solved in the frequency domain in the interaction picture and included the frequency dependence of the effective area as detailed in [43]. A wavelength dependent Kerr coefficient estimated by Romanova *et al.* [44] was used together with the Raman response measured by Ung and Skorobogatiy [45]. To account for any possible coupling to higher-order modes [46, 47] and coupling between the polarization states [48, 49] only 2/3 of the peak power was used in the simulations compared to the experiments.

#221338 - $15.00 USD Received 3 Dec 2014; revised 15 Jan 2015; accepted 28 Jan 2015; published 4 Feb 2015

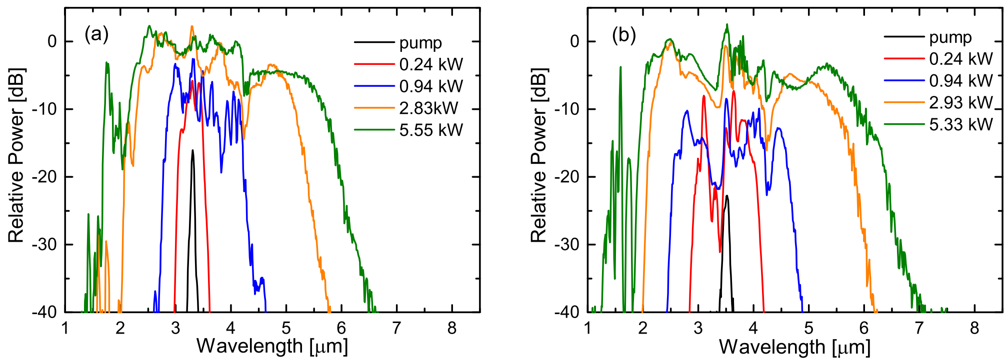

Fig. 3. Pumping at different input powers at (a) 3.3 μm and (b) 3.5 μm. The given powers are the estimated peak power delivered to the fiber.

Figure 4 summarizes the experiments and simulations for varying pump wavelengths up to 4.7 μm. In the experiments we attempted to keep the input peak powers at the different pump wavelengths constant, however, because of different coupling efficiencies the input peak powers varied from 5.3 to 5.7 kW.

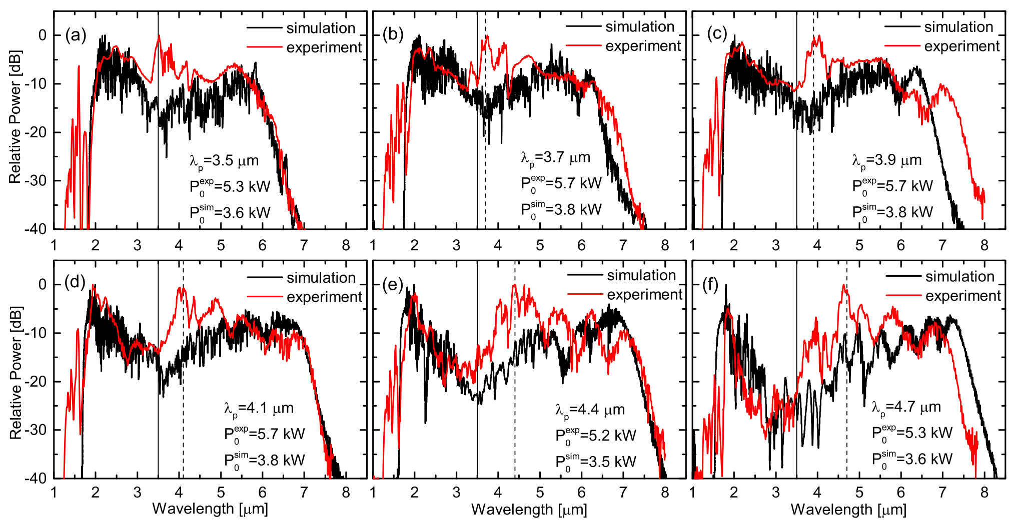

Fig. 4. Comparison between simulations (black) and experiments (red) at six different pump wavelengths (vertical dotted line). The ZDW is indicated as the vertical solid line.

When the pump wavelength was shifted from 3.5 to 4.7 μm the solitonic long wavelength edge moved to longer wavelengths in the simulated spectra, and accordingly the short wavelength edge, consisting of group-velocity matched dispersive waves was shifted to shorter wavelengths. As a result the broadest numerical spectrum spanning 1.65-7.70 μm was obtained when pumping at 4.7 μm. There was still a good agreement between the numerical and experimental results. However the same clear trend of the long wavelength edge moving to longer wavelengths when pumping at longer wavelengths was not observed in the experiments. In the experiments the supercontinuum spectrum was clearly broadened when the pump was shifted from 3.5 to 3.9 μm, while it was more or less constant with a pump wavelength between 3.9 and 4.7 μm. The absence of a long wavelength extension when pumping at longer wavelengths in

#221338 - $15.00 USD Received 3 Dec 2014; revised 15 Jan 2015; accepted 28 Jan 2015; published 4 Feb 2015

the experiments can be explained by coupling instability, e.g. if coupling to the core is slightly off-centered a larger fraction of the power will be coupled to higher-order modes [47] thereby limiting the broadening process. The broadest experimental supercontinuum spectrum spanning from 1.7 to 7.5 μm was obtained when pumping at 4.4 μm, and the average output power was in this case 15.6 mW with a chalcogenide lens at the fiber output and the chopper off. Based on the spectrum and the average output power we calculated the average power >5.0 μm to be 4.7 mW. When pumping at 4.7 μm parts of the supercontinuum spectrum from 2.0 to 3.5 μm was below -20 dB. Here the average output power was 16.0 mW and with an average power >5.0 μm of 7.5 mW.

4. Numerical investigation of the supercontinuum generation process

The dynamics of SCG is well-known. Nonetheless, we will here make a numerical investigation of the initial SCG broadening process and the influence of the Raman contribution. Figure 5 compares numerically calculated density plots of the supercontinuum spectral and temporal evolution along the fiber length for different input powers pumped at 3.5 μm. The supercontinuum spectrum broadens as the input power is increased and there is a good correspondence between the measured and simulated results. The initial SCG is dominated by

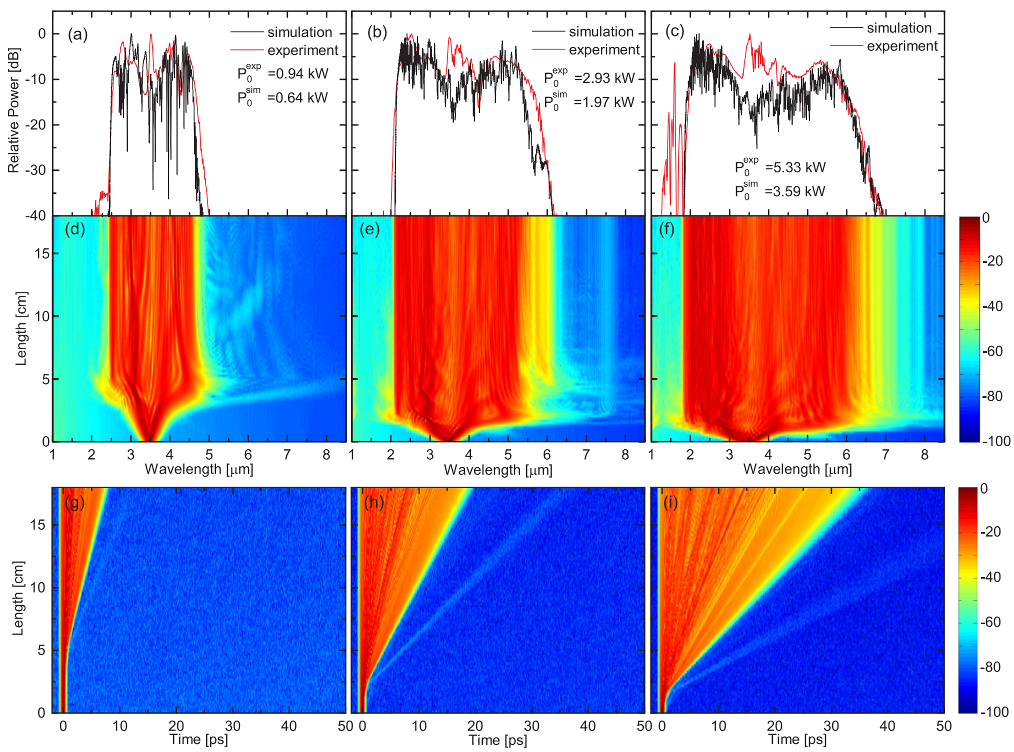

Fig. 5. Comparison between experiments and simulations (5 ensamble average) for three different input powers pumped at 3.5 μm. (a)-(c): Numerical (black) and experimental (red) spectrum after 18 cm of fiber. (d)-(f): Numerical spectral evolution as a function of the fiber length. (g)-(i): Numerical temporal evolution as a function of the fiber length.

self-phase modulation (SPM) indicated by the symmetric (in frequency) spectral broadening and the z-independent temporal profile. The SPM is then followed by soliton dynamics in the

#221338 - $15.00 USD Received 3 Dec 2014; revised 15 Jan 2015; accepted 28 Jan 2015; published 4 Feb 2015

long wavelength part, and the solitonic traces can be observed in the temporal density plots in Figs. 5(g)–5(i).

To verify that the spectral edges in fact are determined by a soliton and corresponding group-velocity matched dispersive waves the group-velocity matched short wavelength edge was determined from the measured long wavelength edge and compared to the measured short wavelength edge at different input powers in Table 1. In all cases there is a good agreement between the measured and the estimated short wavelength edge.

Table 1. Pumping at 3.5 μm. Measured long and short wavelength edges at -20 dB, group-velocity matched short wavelength edges and the short wavelength edge difference at different input peak powers coupled to the fiber.

Peak power	[kW]	0.24	0.47	0.94	1.89	2.93	4.07	5.33
Measured long λ-edge	[μm]	4.11	4.43	4.75	5.25	5.86	6.24	6.34
Measured short λ-edge	[μm]	2.90	2.68	2.49	2.31	2.07	1.96	1.91
GV matched short λ-edge	[μm]	3.03	2.82	2.65	2.42	2.20	2.09	2.06
Short λ-edge difference	[μm]	0.13	0.14	0.16	0.11	0.13	0.13	0.15

From Fig. 5 it can be difficult to determine whether soliton-self-frequency shift (SSFS) is present and influences the broadening process. In Fig. 6 we compare simulations for pumping at 3.5 μm including and excluding the Raman contribution, which is the driving force behind SSFS. Both the temporal and spectral density plots and the spectra in Fig. 6 indicate that SSFS

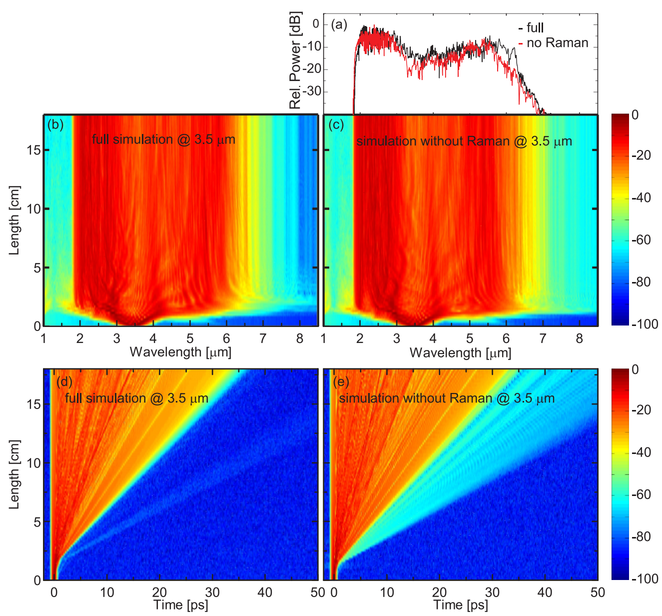

Fig. 6. Simulations with and without Raman contribution pumped at 3.5 μm. (a) Spectra after 18 cm of propagation. (b)-(c) Spectral evolution as a function of fiber length including and excluding the Raman contribution, respectively. (d)-(e) Temporal evolution as a function of fiber length including and excluding the Raman contribution, respectively.

plays a minor role when pumping at 3.5 μm. However, as we move the pump away from the ZDW the dispersion and nonlinearity of the fiber will change. This is illustrated in Fig. 7 where we compare simulations for pumping at 4.4 μm including and excluding the Raman contribution. Again, the supercontinuum broadening process is initiated by SPM. Compared to

#221338 - $15.00 USD Received 3 Dec 2014; revised 15 Jan 2015; accepted 28 Jan 2015; published 4 Feb 2015

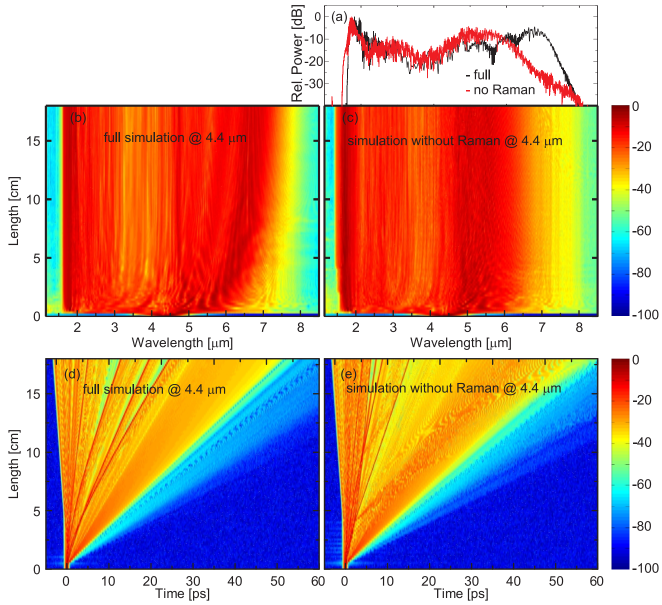

Fig. 7. Simulations with and without Raman contribution pumped at 4.4 μm. (a) Spectra after 18 cm of propagation. (b)-(c) Spectral evolution as a function of fiber length including and excluding the Raman contribution, respectively. (d)-(e) Temporal evolution as a function of fiber length including and excluding the Raman contribution, respectively.

pumping at 3.5 μm the supercontinuum broadens faster and more. Furthermore, SSFS plays a more dominant role, which is clearly seen in the long-wavelength edges of the spectra in Fig. 7(a).

5. Conclusion

We have presented experimental results on SCG in a low-loss $As_{38}Se_{62}$ suspended core fiber with a core diameter of 4.5 μm pumped at different wavelengths from 3.3 to 4.7 μm with 320 fs pulses from an OPA. When pumping at 4.4 μm with a peak power of 5.2 kW coupled to the fiber we obtained a supercontinuum spanning from 1.7-7.5 μm with an average output power of 15.6 mW and an average power $>$5.0 μm of 4.7 mW. The dispersion was measured from 2.9 to 4.2 μm and it was in good correspondence with the calculated dispersion. Simulations based on the generalized nonlinear Schrödinger equation were in good agreement with the measured spectra. Furthermore, simulations confirmed that the SCG was initiated by self-phase modulation, which were the main driving forces, followed by soliton dynamics and soliton self-frequency shift, which increased with increasing pump wavelength in the anomalous dispersion regime.

Acknowledgments

This work has been supported by the European Commission through the Framework Seven (FP7) project MINERVA: MId- to NEaR infrared spectro-scopy for improVed medical di-Agnostics (317803; www.minerva-project.eu); by Innovation Fund Denmark (Light & Food, j.no. 132-2012-3); and by the Australian Research Council Centre of Excellence grant CE110001018. Yi Yu acknowledges the financial support of the China Scholarship Council for PhD Scholarship No.201206110048.